Optics Letters

Tunable switching between stable and periodic states in a semiconductor laser with feedback

Jia-Xin Dong,[1] Jun-Ping Zhuang,[1,2] and Sze-Chun Chan[1,3,*]

[1]Department of Electronic Engineering, City University of Hong Kong, Hong Kong, China
[2]Huawei Technologies Co., Ltd., Shenzhen, China
[3]State Key Laboratory of Millimeter Waves, City University of Hong Kong, Hong Kong, China
*Corresponding author: scchan@cityu.edu.hk

Received 8 August 2017; revised 18 September 2017; accepted 23 September 2017; posted 25 September 2017 (Doc. ID 304253); published 18 October 2017

Feedback-induced switching between two nonlinear dynamical states is observed in a semiconductor laser. The single-mode laser is subject to optical feedback in the long-cavity regime. In every round-trip time τ, the feedback is found to switch the laser from a stable state to a periodic state. The stable state corresponds to a continuous-wave emission at a single optical frequency. The periodic state corresponds to emission at another optical frequency with sidebands generated from a sustained relaxation oscillation. Such regular switching between the stable and periodic states is first unveiled numerically. Experimentally, the resultant intensity time series is confirmed as comprising of a square-wave envelope repeating in τ, which is modulated on a microwave carrier near the relaxation resonance frequency. Additionally, the duty cycle for the periodic state is found as continuously tunable by adjusting the feedback strength. The tunable state switching is applicable to square-wave modulated photonic microwave generation.

OCIS codes: (250.5960) Semiconductor lasers; (190.3100) Instabilities and chaos; (060.5625) Radio frequency photonics.

https://doi.org/10.1364/OL.42.004291

Semiconductor lasers subject to perturbations exhibit a wide range of nonlinear dynamics for the generation of a number of photonic microwave signals [1–4]. The most investigated perturbation is through optical feedback because of the simplicity as well as the high dimensionality [3–16]. Optical feedback induces nonlinear dynamics as in the stable, periodic, quasi-periodic, and chaotic states. The stable state is useful in yielding continuous-wave emission with linewidth reduction [11,17]. The periodic state normally gives regular pulsation at microwave frequencies, where mode-locked pulses were recently obtained using quantum-dot lasers [18,19]. The quasi-periodic state outputs pulses with modulated amplitudes [14,20]. The chaotic state generates broadband microwave signals for niche applications, such as random bit generation, secure communication, and target ranging [21–23]. Also, a state of pulse packages in the short-cavity regime gives pulses of relatively irregular amplitudes, which repeat in packages at the relaxation resonance frequency [24,25]. As for the state of low-frequency fluctuation, a recent real-time frequency analysis disclosed the rapid drifts between the solitary laser mode and fast pulsation modes in different time fragments [26,27].

Optical feedback can also lead to switching between modes in multimode lasers. Polarization-rotated feedback can cause polarization mode switching in edge-emitting lasers and vertical-cavity surface emitting lasers [28–33]. Counter-directional feedback can cause directional mode switching in semiconductor ring lasers [34,35]. Such mode switching forces different modes to emit alternatively, resulting in an intensity time series as square-waves, which are often accompanied by fluctuations or damped relaxation oscillations. It is applicable to optical digital signal processing or clock generation [35,36]. Recently, switching between chaotic and laminar dynamical states was observed in a single-mode laser by using a photonic integrated circuit to realize on-chip feedback [15,16]. However, as a phenomenon of intermittency, the switching does not occur regularly [15,16]. It gives bursts of chaos that are separated by some unpredictable laminar times.

In this Letter, switching between the stable and periodic states is found for a semiconductor laser subject to optical feedback. The switching occurs regularly for the single-mode laser in every feedback round-trip time τ, which is much longer than the reciprocal of the relaxation resonance frequency f_r. The stable state emits in continuous-wave at a single optical frequency, whereas the periodic state emits at another optical frequency with sidebands separated by a frequency f_0 near f_r due to sustained relaxation oscillation. Numerically, the regular switching between the stable and periodic states is first unveiled based on the rate-equation model. Experimentally, the switching results in an emission intensity time series that comprises of a square-wave envelope repeating in τ, which is modulated on a microwave carrier at f_0. In addition, as the feedback strength varies, the periodic state occupies a duty cycle that is continuously tunable. Such tunable state switching is useful for photonic microwave generation with square-wave modulation.

Figure 1 shows the schematic of a single-mode semiconductor laser subject to optical feedback. Light emitted from the laser is launched into a piece of fiber, transmitted from port

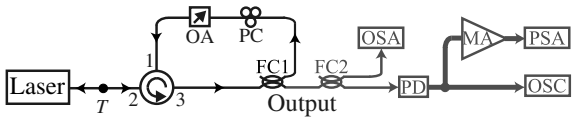

Fig. 1. Schematic of a single-mode semiconductor laser with optical feedback. OA, optical attenuator; PD, photodetector; MA, microwave amplifier; OSC, oscilloscope; PSA, power spectrum analyzer; OSA, optical spectrum analyzer.

2 to 3 of a circulator, coupled through a fiber coupler (FC1), and then fed back via port 1 to 2 of the circulator into the laser. The normalized strength of the feedback field is denoted by ξ, which can be tuned using a variable optical attenuator (OA). The feedback round-trip time is denoted as τ for the emission from the laser to propagate back into the laser. The polarization of the feedback light is adjusted, by a polarization controller (PC), to match that of the laser. Such conventional optical feedback on the laser is known for inducing different nonlinear dynamical states, though not yet known for yielding regular switching between stable and periodic states, as elucidated below.

Numerically, the laser is described by the intracavity field amplitude $a(t)$, in reference to the free-running optical frequency ν_0 of the laser, and the normalized charge carrier density $\tilde{n}(t)$. Its dynamics under feedback in Fig. 1 is governed by the rate equations based on the Lang–Kobayashi model [5,13]:

$$\frac{da}{dt} = \frac{1 - ib}{2}\left[\frac{\gamma_c\gamma_n}{\gamma_s\tilde{J}}\tilde{n} - \gamma_p(|a|^2 - 1)\right]a + \xi\gamma_c a(t-\tau), \quad (1)$$

$$\frac{d\tilde{n}}{dt} = -(\gamma_s + \gamma_n|a|^2)\tilde{n} - \gamma_s\tilde{J}\left(1 - \frac{\gamma_p}{\gamma_c}|a|^2\right)(|a|^2 - 1), \quad (2)$$

where the cavity decay rate $\gamma_c = 5.36 \times 10^{11}$ s^{-1}, the spontaneous carrier relaxation rate $\gamma_s = 5.96 \times 10^9$ s^{-1}, the differential carrier relaxation rate $\gamma_n = 7.53 \times 10^9$ s^{-1}, the nonlinear carrier relaxation rate $\gamma_p = 1.91 \times 10^{10}$ s^{-1}, the linewidth enhancement factor $b = 3.2$, and the normalized bias current above threshold $\tilde{J} = 1.222$ are adopted from a typical semiconductor laser [13]. The optical feedback phase is set at zero for simplicity. The laser has a relaxation resonance frequency f_r of about 10 GHz. Second-order Runge–Kutta integration on Eqs. (1) and (2) with a time step of 1 ps yields the time-varying emission $a(t)$.

Figure 2 shows the optical spectrograms of the laser emission simulated under a feedback strength of $\xi = 0.02$ at different feedback round-trip times τ. Each spectrogram is obtained by applying a short-time Fourier transform with a 0.5 ns Gaussian sliding window on $a(t)$, thereby revealing the real-time evolution of the optical spectrum [18,26]. In Fig. 2(a), with τ of 0.02 ns being much shorter than $1/f_r$, the feedback is in the short-cavity regime. The laser is in a stable state, maintaining a continuous-wave emission at a single optical frequency ν_s, which is 4 GHz below the free-running optical frequency ν_0. The emission is supported by an external cavity mode that is redshifted by the antiguidance effect [13,15]. In Fig. 2(b), τ is increased to 0.2 ns in becoming comparable to $1/f_r$. The laser is no longer stable, but enters a periodic state. The main emission is now at an optical frequency ν_p near ν_0 and is accompanied by sidebands separated by $f_0 = 8.8$ GHz. The sidebands stem from undamping the relaxation oscillation

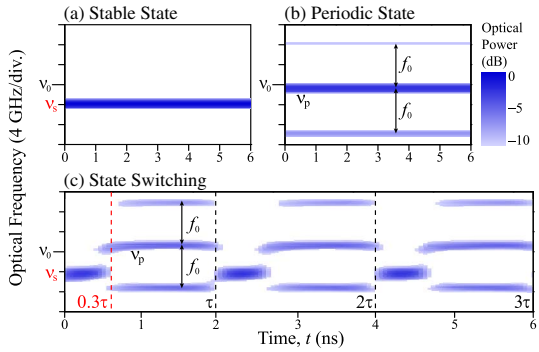

Fig. 2. Optical spectrogram of the laser emission obtained in (a) stable state, (b) periodic state, and (c) state switching when the feedback round-trip time $\tau = 0.02$ ns, 0.2 ns, and 2 ns, respectively. The feedback strength is kept constant at $\xi = 0.02$.

at f_r into a sustained periodic oscillation at the slightly shifted f_0 [6,13]. As for Fig. 2(c) with τ further increased to 2 ns, the feedback induces switching between the stable and periodic states. The feedback is in the long-cavity regime with τ being much longer than $1/f_r$. From time $t = 0$ to 0.3τ, the spectrogram initially shows the stable state emitting only at ν_s. From $t = 0.3\tau$ to τ, a switch to the periodic state is observed with an emission at ν_p accompanied by sidebands separated by f_0. The frequency components start to strengthen nearly simultaneously and are then maintained over the duration of 0.7τ. Then, at $t = \tau$, the initial emission at ν_s is fed back to the laser, forcing the laser to return to the stable state at ν_s. The switching between the stable and periodic states continues regularly in every τ. Essentially, the state switching is much more regular when compared to the irregular intermittencies or low-frequency fluctuations [16,27]. The switching of states within a feedback round-trip time resembles the interesting chimera states, which have been studied in optoelectronic oscillators with electronic feedback [37,38]. Nonetheless, for single-mode lasers with optical feedback, Fig. 2(c) first reveals the regular switching between the stable and periodic states. It is generally possible in the simulation with $\tau > 1$ ns. The optical frequency components are dependent on the parameters of the feedback and the laser. The following focuses on regular switching between stable and periodic states.

Experimentally, Fig. 1 is implemented using a 1.55 μm single-mode distributed-feedback laser (FITEL FRL15DCW5-A81-19327). The laser has a threshold of 10 mA when temperature-stabilized at 21°C. It has a relaxation resonance frequency of approximately $f_r = 10$ GHz when biased at 50 mA. The laser is coupled with a packaged fiber pigtail with a nominal coupling efficiency of 0.5, emitting about 9 mW at the end of the pigtail at position T. After the circulator, FC1 splits 70% of the power for passing through the attenuator OA, so that about 86 μW returns to T for feeding back into the laser. The feedback polarization is matched to the laser by adjusting PC as indicated by its threshold reduction [39]. So the feedback strength ξ, proportional to the feedback field amplitude at the laser, is estimated as 0.024 [13]. The feedback round-trip time τ in the experiment is about 63 ns in the long-cavity regime. For detection, FC1 sends the remaining 30% of the laser emission as the output through a 50:50 fiber

coupler (FC2) to an optical spectrum analyzer (YOKOGAWA AQ6370) and to a photodetector (PD), which actually comprises an erbium-doped fiber preamplifier connected to a 50 GHz detector (u2t XPDV2120RA). The electrical output of PD is split for monitoring by a 12 GHz real-time oscilloscope (Agilent DSO90254A) and by a power spectrum analyzer (Agilent N9010A) with a microwave amplifier (Agilent 83006A). In practice, using a slower dc-coupled detector (Thorlabs DET01CFC), the high-speed ac-coupled PD is calibrated for the offset and responsivity at the oscilloscope.

Figures 3 and 4 experimentally demonstrate the switching between stable and periodic states. In Fig. 3(a), the optical spectrum is shown around the free-running optical frequency $\nu_0 =$ 193.47 THz of the laser. It is recorded by the optical spectrum analyzer in Fig. 1 with a sweep time of 1 s and a limited resolution bandwidth of 2.5 GHz. On one hand, the spectrum in Fig. 3(a) has a strong component at ν_s, of about 3 GHz below ν_0. The component is attributed to a stable state. On the other hand, the spectrum also has a relatively strong component at ν_p of about 2 GHz above ν_0, where the next strongest components are at $\nu_p - f_0$ and then at $\nu_p + f_0$ with $f_0 = 8.36$ GHz in the experiment. There are a number of sidebands separated by multiples of f_0 around ν_p, as indicated by the dashed lines in Fig. 3(a), which are attributed to a periodic state. Similarly to Fig. 2(c), the optical spectrum in Fig. 3(a) comprises of the component at ν_s for the stable state and the components at ν_p with sidebands separated by multiples of f_0 for the periodic state. Both the stable state and the periodic state contribute to Fig. 3(a) because the sweep time of the optical spectrum analyzer is much slower than τ.

Although the experimental optical spectrum in Fig. 3(a) lacks temporal resolution, the temporal switching of the optical frequency components can be deduced from the corresponding power spectrum in Fig. 3(b). Due to the beating of ν_p and its sidebands separated by f_0 in Fig. 3(a), the power spectrum in Fig. 3(b) peaks at f_0 and its harmonics. The power spectrum in Fig. 3(b) does not have any strong peak at $\nu_p - \nu_s \approx 5$ GHz, indicating the absence of beating between the optical frequency components at ν_s and ν_p, which implies the lack of temporal overlap for the emissions at ν_s and ν_p. In other words, Fig. 3(b) indicates that the laser alternatively switches between the stable state at ν_s and the periodic state at ν_p with sidebands. Also, the power spectrum is recorded in a zoomed frequency range around the microwave carrier at f_0 in Fig. 3(c). There are discrete frequency components equally separated by $1/\tau =$ 16 MHz, which corresponds to the frequency of the switching.

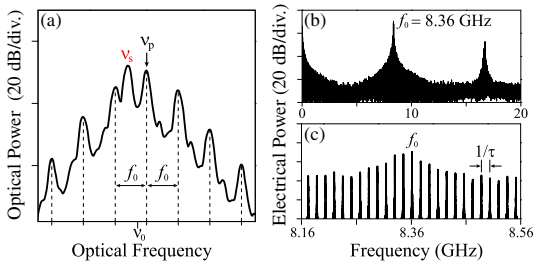

Fig. 3. (a) Optical spectrum, (b) power spectrum, and (c) zoomed power spectrum of the laser in state switching. The laser switches between a stable state at ν_s and a periodic state at ν_p with sidebands separated by f_0. Feedback of $\xi = 0.024$ and $\tau = 63$ ns is used.

The linewidths of the microwave carrier at f_0 and its sidebands separated by $1/\tau$ are measured to be less than 25 kHz, as the switching occurs regularly in every τ. Such a spectrum comprising of discrete components from the frequency mixing of f_0 and $1/\tau$ is often observed in quasi-periodic dynamics [9,15]. The regular switching between the stable and periodic states in Fig. 3 is more directly recorded by the associated intensity time series.

Figure 4 shows the time series as normalized to the free-running intensity of the laser. The feedback strength ξ is set at 0.024, 0.026, and 0.027 for Figs. 4(a), 4(b), and 4(c), respectively, with a constant $\tau = 63$ ns. Whereas column (i) has a time span of 3τ, column (ii) is zoomed to a much smaller span as the state switches. For Fig. 4(a) with ξ of 0.024, the time series corresponds to the spectra in Fig. 3. From time $t = 0$ to about 0.5τ, Fig. 4(a-i) shows a nearly constant intensity at around 1, as indicative of the stable state. From $t = 0.5\tau$ to τ, the laser is switched to the periodic state as the intensity becomes oscillatory in Fig. 4(a-i), where the oscillation at $f_0 = 8.36$ GHz is observed in Fig. 4(a-ii). The intensity periodically varies between 1.12 and 0.92 in yielding an oscillation amplitude of 0.2. Such an oscillation corresponds to the peak at f_0 in Fig. 3(b) that is mainly due to the beating of the optical frequency components at ν_p and $\nu_p - f_0$ in Fig. 3(a). Then, the switching between the stable and periodic states repeats regularly in every τ, where the periodic state occupies a duty cycle of 0.5 in Fig. 4(a). The experimental results in Fig. 4 qualitatively agree with the numerical results in Fig. 2(c), demonstrating the regular switching between the stable and periodic states. Practically, the state switching generates the intensity time series with the microwave carrier at f_0 that is modulated by a square-wave envelope repeating in τ. The result can be viewed as quasi-periodicity because the oscillatory carrier is modulated by an envelope [40].

State switching continues to be observed in Fig. 4(b) as ξ increases to 0.026, where the stable state switches to the periodic state at $t = 0.7\tau$ in yielding a reduced duty cycle of 0.3 for the periodic oscillation. In Fig. 4(c) as ξ increases to 0.027, the switch to the periodic state is postponed to $t = 0.9\tau$ for a further reduced duty cycle of 0.1. State switching enables not only square-wave modulated photonic microwave generation [2,14], but also a continuous tuning of the duty cycle.

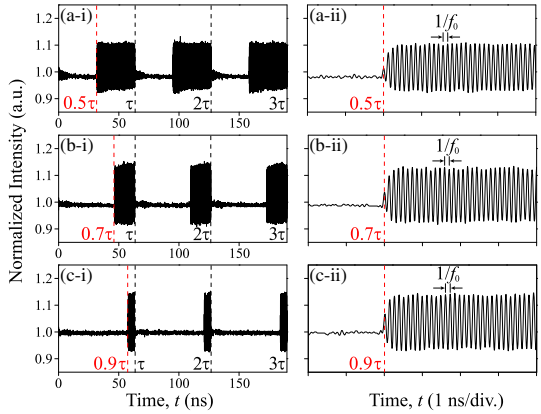

Fig. 4. (i) Intensity time series and (ii) zoomed intensity time series of the laser in state switching. The laser switches between a stable state and a periodic state oscillating at f_0. The feedback strength ξ = (a) 0.024, (b) 0.026, and (c) 0.027, while $\tau = 63$ ns.

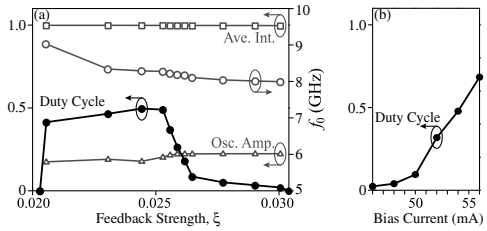

Fig. 5. (a) Duty cycle, average intensity, amplitude, and frequency of the periodic oscillation as functions of ξ during state switching at a bias of 50 mA. (b) Duty cycle versus bias at $\xi = 0.026$.

Figure 5(a) plots the duty cycle (in closed circles) versus the feedback strength ξ. For small ξ, the laser remains solely in the stable state without any switching, so the duty cycle for the periodic state is zero. By increasing ξ beyond 0.020, the laser starts to exhibit switching between stable and periodic states. The duty cycle for the periodic state increases to 0.5 when ξ reaches 0.024, as in Fig. 4(a-i). A continual increase of ξ eventually results in a continuous reduction of the duty cycle in Fig. 5(a). The duty cycle returns to zero at ξ of around 0.030 as the laser returns to the stable state without switching. Thus, in state switching, the periodic state occupies a duty cycle that is continuously tunable between 0.5 and 0 by varying ξ at a fixed bias current of 50 mA. A wider tuning range is possible when the bias is adjusted in Fig. 5(b) at $\xi = 0.026$. For completeness, the squares in Fig. 5(a) plot the time-averaged normalized intensity of the laser, which remains nearly independent of ξ because of the relatively weak feedback. The triangles then show a nearly constant oscillation amplitude for the periodic state, though the associated oscillation frequency f_0 (in open circles) gradually reduces when ξ increases. In any case, state switching is observed only over a narrow range of ξ from 0.020 to 0.030, as both stable and periodic states have to be supported by the feedback alternatively.

To summarize, state switching in a semiconductor laser with feedback is unveiled both numerically and experimentally. The feedback induces regular switching between the stable and periodic states in the long-cavity regime. The resultant intensity time series contains a square-wave envelope that is repeating in the feedback round-trip time τ and is modulated on a microwave carrier at f_0 near the relaxation resonance frequency of the laser, where the periodic state occupies a continuously tunable duty cycle. Such a tunable state switching can be of interest in square-wave modulated photonic microwave generation.

Funding. Research Grants Council, University Grants Committee (RGC, UGC) (CityU 11201014, CityU 11260916, T42-103/16-N).

REFERENCES

1. M. Sciamanna and K. A. Shore, Nat. Photonics **9**, 151 (2015).
2. T. B. Simpson, J. M. Liu, M. AlMulla, N. G. Usechak, and V. Kovanis, Phys. Rev. Lett. **112**, 023901 (2014).
3. M. C. Soriano, J. Garca-Ojalvo, C. R. Mirasso, and I. Fischer, Rev. Mod. Phys. **85**, 421 (2013).
4. A. Uchida, K. Amano, M. Inoue, K. Hirano, S. Naito, H. Someya, I. Oowada, T. Kurashige, M. Shiki, S. Yoshimori, K. Yoshimura, and P. Davis, Nat. Photonics **2**, 728 (2008).
5. R. Lang and K. Kobayashi, IEEE J. Quantum Electron. **16**, 347 (1980).
6. J. Mork, B. Tromborg, and J. Mark, IEEE J. Quantum Electron. **28**, 93 (1992).
7. K. Petermann, IEEE J. Sel. Top. Quantum Electron. **1**, 480 (1995).
8. M. Yousefi, D. Lenstra, and G. Vemuri, Phys. Rev. E **67**, 046213 (2003).
9. S. G. Abdulrhmann, M. Ahmed, T. Okamoto, W. Ishimori, and M. Yamada, IEEE J. Sel. Top. Quantum Electron. **9**, 1265 (2003).
10. D. Rontani, A. Locquet, M. Sciamanna, and D. S. Citrin, Opt. Lett. **32**, 2960 (2007).
11. S. Donati and R. H. Horng, IEEE J. Sel. Top. Quantum Electron. **19**, 1500309 (2013).
12. C. F. Chuang, Y. H. Liao, C. H. Lin, S. Y. Chen, F. Grillot, and F. Y. Lin, Opt. Express **22**, 5651 (2014).
13. S. S. Li and S. C. Chan, IEEE J. Sel. Top. Quantum Electron. **21**, 541 (2015).
14. C. Y. Chang, D. Choi, A. Locquet, M. J. Wishon, K. Merghem, A. Ramdane, F. Lelarge, A. Martinez, and D. S. Citrin, Appl. Phys. Lett. **108**, 191109 (2016).
15. A. K. Dal Bosco, Y. Akizawa, K. Kanno, A. Uchida, T. Harayama, and K. Yoshimura, Opt. Express **24**, 22198 (2016).
16. A. K. Dal Bosco, N. Sato, Y. Terashima, S. Ohara, A. Uchida, T. Harayama, and M. Inubushi, IEEE J. Sel. Top. Quantum Electron. **23**, 1801208 (2017).
17. D. Brunner, R. Luna, A. D. i Latorre, X. Porte, and I. Fischer, Opt. Lett. **42**, 163 (2017).
18. J. P. Zhuang, X. Z. Li, S. S. Li, and S. C. Chan, Opt. Lett. **41**, 5764 (2016).
19. B. Tykalewicz, D. Goulding, S. P. Hegarty, G. Huyet, T. Erneux, B. Kelleher, and E. A. Viktorov, Opt. Express **24**, 4239 (2016).
20. F. Y. Lin and J. M. Liu, Appl. Phys. Lett. **81**, 3128 (2002).
21. R. Sakuraba, K. Iwakawa, K. Kanno, and A. Uchida, Opt. Express **23**, 1470 (2015).
22. V. Annovazzi-Lodi and G. Aromataris, IEEE J. Quantum Electron. **51**, 1 (2015).
23. C. H. Cheng, Y. C. Chen, and F. Y. Lin, IEEE Photon. J. **8**, 7800209 (2016).
24. T. Heil, I. Fischer, W. Elsäßer, and A. Gavrielides, Phys. Rev. Lett. **87**, 243901 (2001).
25. A. Tabaka, K. Panajotov, I. Veretennicoff, and M. Sciamanna, Phys. Rev. E **70**, 036211 (2004).
26. D. Brunner, X. Porte, M. C. Soriano, and I. Fischer, Sci. Rep. **2**, 732 (2012).
27. D. Brunner, M. C. Soriano, X. Porte, and I. Fischer, Phys. Rev. Lett. **115**, 053901 (2015).
28. A. Gavrielides, D. W. Sukow, G. Burner, T. McLachlan, J. Miller, and J. Amonette, Phys. Rev. E **81**, 056209 (2010).
29. R. Ju and P. S. Spencer, J. Lightwave Technol. **23**, 2513 (2005).
30. T. Heil, A. Uchida, P. Davis, and T. Aida, Phys. Rev. A **68**, 033811 (2003).
31. C. Masoller, D. Sukow, A. Gavrielides, and M. Sciamanna, Phys. Rev. A **84**, 023838 (2011).
32. G. Friart, G. Verschaffelt, J. Danckaert, and T. Erneux, Opt. Lett. **39**, 6098 (2014).
33. D. W. Sukow, T. Gilfillan, B. Pope, M. S. Torre, A. Gavrielides, and C. Masoller, Phys. Rev. A **86**, 033818 (2012).
34. L. Mashal, G. Van der Sande, L. Gelens, J. Danckaert, and G. Verschaffelt, Opt. Express **20**, 22503 (2012).
35. S. S. Li, X. Z. Li, J. P. Zhuang, G. Mezosi, M. Sorel, and S. C. Chan, Opt. Lett. **41**, 812 (2016).
36. A. Trita, G. Mezosi, M. J. Latorre-Vidal, M. Zanola, M. J. Strain, F. Bragheri, M. Sorel, and G. Giuliani, IEEE J. Quantum Electron. **49**, 877 (2013).
37. A. F. Talla, R. Martinenghi, P. Woafo, and Y. K. Chembo, IEEE Photon. J. **8**, 1 (2016).
38. L. Larger, B. Penkovsky, and Y. Maistrenko, Nat. Commun. **6**, 7752 (2015).
39. J. P. Zhuang and S. C. Chan, Opt. Lett. **38**, 344 (2013).
40. F. Y. Lin and J. M. Liu, IEEE J. Quantum Electron. **39**, 562 (2003).